Multivariate and predictive modelling of neural variability in mild cognitive impairment

Valeria Kebets[1,2], Mitsouko van Assche[1], Jonas Richiardi[3], Rachel Goldstein[4], Reto Meuli[3], Tobias Kober[3], Frédéric Assal[4], Dimitri Van De Ville[5,6]

[1]*Department of Clinical Neuroscience, University of Geneva, Geneva, Switzerland*
[2]*SINAPSE, National University of Singapore, Singapore, Singapore*
[3]*Department of Radiology, Lausanne University Hospital, Lausanne, Switzerland*
[4]*Department of Neurology, Geneva University Hospital, Geneva, Switzerland*
[5]*Institute of Bioengineering, Ecole Polytechnique Fédérale de Lausanne, Lausanne, Switzerland*
[6]*Department of Radiology, University of Geneva, Geneva, Switzerland*

***Abstract*—Brain signal variability has been proposed as an index of the brain's cognitive capacity. In this work, we examined neural variability by calculating the standard deviation of single trial activation estimates during memory encoding in 30 patients with mild cognitive impairment (MCI) and 31 elderly controls. We deployed a random forest (RF) classifier, using variability maps as features to distinguish MCI patients from controls, and obtained classification accuracies of up to 86%. We then used partial least squares correlation to identify variability patterns associated with task performance and compared them to the weight maps obtained with the RF classifier.**

Keywords—Trial-by-trial activation variability; memory encoding; mild cognitive impairment; classification; partial least squares.

I. Introduction

A growing number of studies have recently shown that the brain signal *variance* could provide substantial information about the brain function [1]. Interestingly, it has been proposed that an optimal level of variability (or instability) is required for the brain to adapt to various environmental demands [2]. Within-subject brain signal variability has been associated with individual differences in cognitive performance in young and elderly healthy individuals [3][4]. However, some regions have shown a negative association between neural variability and cognitive performance [5]; furthermore, the benefits of neural variability may depend on the nature of the task [6].

In Alzheimer's disease (AD) and its prodromal stage, mild cognitive impairment (MCI), changes in the amplitude of low-frequency fluctuations (ALFF) at rest were found to be correlated with cognitive performance (Mini-Mental State Examination [MMSE] score) [7]. However, no study to this date has examined neural variability in MCI or AD patients during a memory task.

We computed trial-by-trial functional magnetic resonance imaging (fMRI) activation variability during memory encoding, and used these variability maps as features for the individual classification of MCI patients and healthy controls (HC). Furthermore, we used partial least squares (PLS) to identify patterns of neural variability associated with recognition performance. We assessed the reliability of this association by computing PLS in a cross-validation scheme. Finally, we also investigated the impact of "block normalization" (a processing step applied in [2], similar to global signal regression) when computing brain signal variability, on both PLS and classification results.

II. Material and Methods

2.1 Subjects

Thirty amnestic MCI patients (both single- and multiple-domain) and 31 elderly HC participated in this study (**Table I**). All participants completed a battery of standardized neuropsychological tests assessing general cognitive function, memory, language and executive functions. MCI diagnosis was based on Petersen's criteria [8]. HC were to have a normal neurological and neuropsychological examination, and no significant cognitive complaint. The study was approved by the local ethics committee, and written informed consent was obtained from all participants.

2.2 MRI acquisition

MRI data were acquired on two scanners, both 3T Siemens Trio Tim, using a 12-channel head coil, and identical imaging parameters. Whole brain fMRI images were collected using a susceptibility weighted EPI sequence (TR/TE=1810/30ms; flip angle=90 degrees; PAT factor=2; FOV=192mm; matrix size=64 × 64 pixels). Thirty-two transversal slices were acquired sequentially with a 4mm thickness and an interslice gap of 11mm, yielding a voxel size of 3 × 3 × 5mm. High resolution whole brain anatomical scans were acquired with a T1-weighted 3D sequence (MPRAGE; TR/TI/TE=1900/900/2.32ms; flip angle=9 degrees; voxel dimensions=0.9mm isotropic; 256 × 256 × 192 voxels).

2.3 fMRI memory task

We used a non-verbal associative memory task (see [9] for details about the experimental paradigm). Encoding and recognition phases were alternatively conducted in 3 successive

978-1-5386-6859-7/18/$31.00 ©20XX IEEE

runs. Subjects were first asked to memorize pairs of pictures and press a button to acknowledge their encoding of each pair; they were then presented with a cue picture along with two pictures (the target picture and a distractor), and had to indicate the picture that had been previously paired with the cue picture. There were 24 trials per run (72 in total), on which patients scored significant worse than HC (see **Table I**).

2.4 fMRI data preprocessing

Functional images were preprocessed using SPM12 (http://www.fil.ion.ucl.ac.uk/spm/software/spm12/). Images were first slice-time corrected and realigned. The mean functional image was then co-registered with the anatomical scan. Functional images were normalized to the MNI space with SPM12 Segmentation, then resampled to 3mm isotropic voxels, and smoothed using an 8mm full-width-at-half-maximum Gaussian kernel.

2.5 First-level general linear model

For each subject, we used a first-level general linear model that considered only correct trials, i.e., encoding trials that were subsequently correctly recognized. We used a model known as the multi-regressor approach (based on [10], https://github.com/ritcheym/fmri_misc/blob/master/generate_spm_singletrial.m), whereby each trial is represented by an individual regressor. The model thus included a separate regressor for each trial, resulting in 72 encoding and 72 recognition regressors, to which we added the Friston 24 motion parameters [11]. We also added regressors to model the instructions display before each trial, as well 3 constants to model inter-run variability. All regressors were convolved with the canonical hemodynamic response function. A high-pass filter (with a cut-off frequency of 1/128 seconds) and a first-order autoregressive function (to account for temporal autocorrelation) were included in the fitting procedure. Only betas of the encoding trials were used in our analyses.

2.6 Trial-by-trial activation variability

We first generated a DARTEL [12] group template (using all subjects' anatomical scans) that included all voxels with a grey matter probability ≥ 0.3, resulting in a mask containing M = 33'327 voxels. We computed trial-by-trial activation variability using the betas of the encoding trials, constrained to voxels that fell inside the template. For each subject, after concatenating all betas into a vector of size M × betas, we calculated the standard deviation for each voxel across betas. Variability values were then z-scored across all voxels, for each subject.

Some of the previous studies (e.g., [2]) have applied a "block normalization" procedure to correct for block offsets, which consists in removing global signal within each block. In the present case, each beta was considered as a "block", since the task was event-related. To test whether this procedure would influence our results, we followed a similar procedure to create a second set of variability maps: for each beta, we removed the average signal (extracted within the group template) from each voxel, before concatenating all betas, after which we calculated the standard deviation for each voxel and applied spatial z-scoring. In the remainder of the paper, we refer to these maps as VarNoBN (without block normalization) and VarBN (with block normalization).

TABLE I. SOCIODEMOGRAPHIC DATA AND COGNITIVE PERFORMANCE

	Controls	**MCI patients**	**p-value**
N	31	30	
Age	68.94 (5.85)	71.77 (6.60)	0.081
Gender (F/M)	23 / 8	16 / 14	0.090
Education	14.00 (2.76)	13.23 (3.21)	0.321
Scanner (1/2)	7 / 24	4 / 26	0.348
MMSE	28.32 (1.66)	25.83 (2.10)	<0.001
Task accuracy (%)	94.98 (5.14)	77.36 (10.64)	<0.001

Mean (SD) are shown for all continuous variables. P-values assess the significance of t-tests or χ^2 tests.

2.7 Classification

We used a random forest (RF, [13]) classifier (featuring 501 trees), as implemented in Matlab (https://code.google.com/archive/p/randomforest-matlab/) to discriminate between MCI patients and HC. VarBN and VarNoBN maps were used as features, yielding for each subject a feature vector of size M × 1. In order to evaluate the generalizability of the classifier's performance, we trained the classifier on 29 MCI and 29 HC, and tested it on 1 MCI and 2 HC). We used permutation testing (1'000) to assess the significance of our prediction accuracies, and computed Gini importance [13] to generate weight maps showing the relative contribution of each voxel to the classifier's performance. Finally, we used the McNemar test to assess whether the classifier's performance was significantly different between the two sets of variability maps (VarBN and VarNoBN).

2.8 Partial least squares analysis

PLS is a multivariate data-driven statistical technique that aims to find the optimal relationship between two data matrices by deriving latent variables (LVs) which are weighted linear combinations of the original data that maximally covary with each other [14]. Here, we used PLS to identify trial-by-trial activation variability patterns that are optimally related to task accuracy (computing separate PLS models for VarBN and VarNoBN). In our data, **X** is the imaging matrix (subjects × M), and **Y** contains task accuracy values (subjects × 1).

2.8.1 Original PLS model

After z-scoring **X** and **Y** within each diagnostic group (HC/MCI), we computed a cross-covariance matrix between each pair of matrices (**X** and **Y** for each group), both of size 1 × M. We then concatenated the group-specific cross-covariance matrices into a matrix **R** (of size 2 × M). We followed with singular value decomposition (SVD) of **R**, which provides the best reconstruction of **R** (in a least square sense) by low-dimensional matrices: $\mathbf{R} = \mathbf{U} \times \mathbf{S} \times \mathbf{V}^{\mathbf{T}}$. This decomposition resulted in two mutually orthogonal LVs, of which **U** and **V** are the singular vectors (called respectively *behavior* and *brain saliences*), while **S** is a diagonal matrix containing the singular values. The saliences indicate the contribution of each behavioral measure and each voxel to the brain-behavior correlation explained by the LV. Subjects' imaging and

behavioral contribution to each LV were represented by *brain* and *behavior scores*, and were computed by projecting **X** and **Y** onto their respective saliences **V** and **U**: $\mathbf{L_x} = \mathbf{X} \times \mathbf{V}$, and $\mathbf{L_y} = \mathbf{Y} \times \mathbf{U}$. We assessed the statistical significance of each LV by constructing a null distribution of the singular values using permutation testing (5'000 permutations). In order to evaluate the stability of brain saliences, we used a bootstrapping procedure (1'000 random samples with replacement), generating a set of resampled covariance matrices that were subjected to SVD, and resulting in a sampling distribution of the salience values. We calculated a "bootstrap ratio" (BSR) for each voxel by dividing its brain salience by its bootstrap-estimated standard error.

2.8.2 Cross-validated PLS model

We tested the robustness of our PLS model by applying the same cross-validation scheme as for classification (training on 29 MCI and 29 HC, and testing on 1 MCI and 2 HC). We computed PLS on the training data as described above (without assessing the significance of LVs with permutation testing, but with bootstrap resampling with 100 random samples). Within each fold, after z-scoring the test data (using the mean and standard deviation of the training data), we projected the test data on the brain and behavior saliences of the training data to obtain brain and behavior scores: $\mathbf{L}_{x\ test} = \mathbf{X}_{test} \times \mathbf{V}_{train}$, and $\mathbf{L}_{y\ test} = \mathbf{Y}_{test} \times \mathbf{U}_{train}$. We computed Pearson correlations between $\mathbf{L}_{x\ train}$ and $\mathbf{L}_{y\ train}$ for each fold, and then averaged these correlations across all folds. To evaluate whether these associations were generalizable, we also computed Pearson correlations between $\mathbf{L}_{x\ test}$ and $\mathbf{L}_{y\ test}$ across all folds. These correlations were then compared to those in the original PLS model.

III. Results

3.1 Classification

Prediction accuracies obtained using VarBN and VarNoBN maps can be found in **Table II**. Accuracy was significantly higher when using VarBN maps as features compared to VarNoBN maps (discrepancy of 18.15 between expected and observed counts of error). Weight maps showing the relative contribution of each voxel to the classifier's performance are shown in **Fig 1**. In both models, variability in the precuneus, bilateral hippocampus (HIP), left superior parietal lobule, left superior temporal gyrus and frontal regions were among the regions that most contributed to distinguish between MCI and HC. For VarBN, variability in the anterior cingulate cortex and superior frontal gyrus also highly contributed to the prediction (relative to other voxels).

TABLE II. Classification Performance

	Accuracy	**Specificity**	**Sensitivity**	**p-value**
VarNoBN	74%	74%	76%	0.001
VarBN	86%	90%	78%	0.001

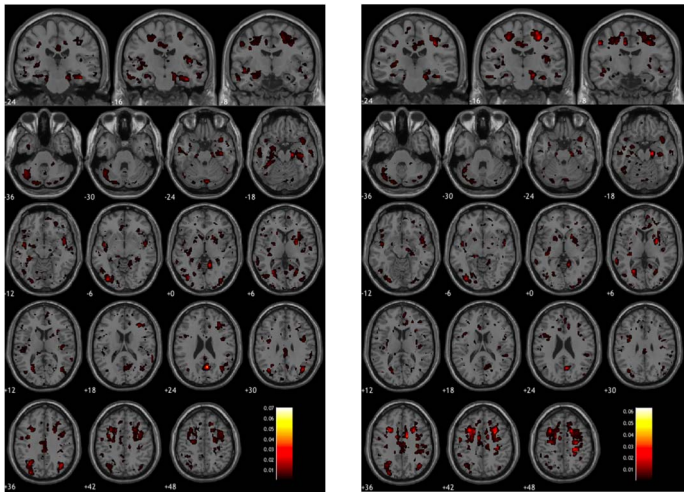

Fig. 1. Weight maps for classifying controls vs. patients using VarNoBN (left) and VarBN (right) maps as features. *Higher values represent higher Gini importance.*

3.2 Original PLS model

We obtained very similar results with both PLS models. The first LV was significant (r=0.81, permuted p=0.002 using VarNoBN, and r=0.76, permuted p=0.047 using VarBN). Interestingly, the association between neural variability and task performance was driven by MCI patients, in whom correlations were more than twice higher than in HC (see **Table III**). Performance-related spatial patterns were almost identical between the two models (**Fig 2**): task performance was correlated with increased variability in the left HIP, left temporal pole, posterior cingulate cortex (PCC), medial prefrontal cortex (mPFC), and with decreased variability in fronto-parietal regions.

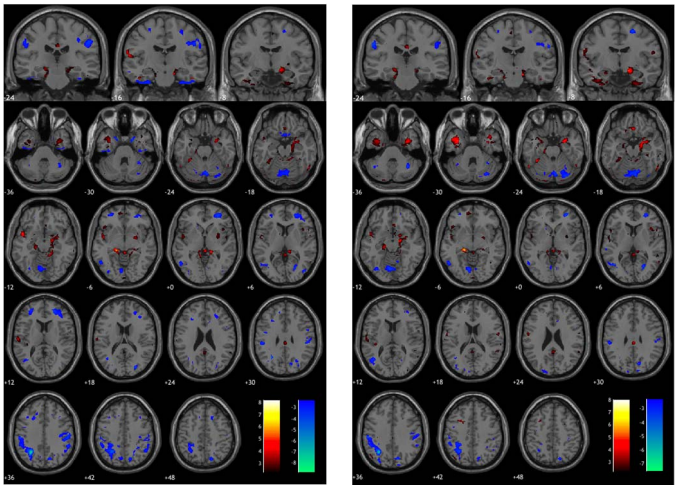

Fig. 2. PLS brain pattern bootstrap ratio for the original PLS model, using VarNoBN (left) and VarBN (right) maps. Both maps were thresholded at 2.3, which corresponds to p~0.05. *Regions in red are positively correlated with task accuracy, while regions in blue show a negative correlation.*

3.3 Cross-validated PLS model

Correlations between $\mathbf{L}_x$ and $\mathbf{L}_y$ for training and test sets can be found in **Table III**. While they were stable across training sets, these correlations dropped drastically in test sets, especially for the model with VarBN.

TABLE III. COMPARISON BETWEEN ORIGINAL AND CROSS-VALIDATED PLS MODELS

VarNoBN		**VarBN**	
	Corr L_x-L_y		***Corr L_x-L_y***
Original model		*Original model*	
In HC	0.40 (p=0.026)	In HC	0.34 (p=0.063)
In MCI	0.86 (p=0.000)	In MCI	0.88 (p=0.000)
*Training sets**		*Training sets**	
In HC	0.39 (0.10)	In HC	0.32 (0.18)
In MCI	0.86 (0.01)	In MCI	0.88 (0.01)
Test sets		*Test sets*	
In HC	0.16 (p=0.111)	In HC	-0.04(p=0.666)
In MCI	0.18 (p=0.077)	In MCI	0.02 (p=0.856)

*Correlations and behavior saliences were averaged across training sets; mean (SD) values are shown.

IV. DISCUSSION

We found that trial-by-trial activation variability during memory encoding allowed to discriminate MCI patients from controls. Interestingly, the block normalization procedure significantly improved the classifier's performance; thus, by removing low frequency drifts and reducing voxel variance, this preprocessing step also increased group discriminability.

Moreover, neural variability was strongly related to task performance, in line with previous reports [3][5][6]. This relationship was stable across training sets; however, the correlations were much lower when tested on unseen data. However, we note that unsupervised models such as PLS are not commonly tested via cross-validation, as their value lies in the exploratory analysis of associations between data set.

Performance-related patterns of variability were bidirectional, and most of the patterns in fact showed a *negative* association with performance. Interestingly, the default mode network (DMN) – a group of regions that is affected early in the course of AD - was divided into a ventral part (HIP, lateral temporal cortex, mPFC, PCC) in which neural variability was beneficial, and a dorsal part (precuneus, lateral parietal cortex) in which it was detrimental for task performance. High neural variability in the mPFC and PCC has been shown to correlate with better performance in healthy subjects [3][6]; however, variability in the HIP has shown the opposite association [15]. Finally, variability in the DMN and in fronto-parietal regions – overlapping with regions associated with task performance – contributed to distinguish MCI patients from controls. Our results therefore add to the evidence that neural variability is indeed a signal of interest that should be considered in future studies.

Among the limitations of this work, we note that the use of a DARTEL template may have induced knowledge about test sets during training; in addition, the small sample size may limit the generalizability of our findings.

ACKNOWLEDGMENT

This work was supported by the Swiss National Science Foundation (FNS 320030_138163), Louis Jeantet Foundation (ME 10244), Ernest Boninchi Foundation (ME 10376), and Société Académique de Genève (NAC 08-025). The work of our group is supported by the Singapore MOE Tier 2 (MOE2014-T2-2-016), NUS Strategic Research (DPRT/944/09/14), NUS SOM Aspiration Fund (R185000271720), Singapore NMRC (CBRG/0088/2015), NUS YIA and the Singapore National Research Foundation (NRF) Fellowship (Class of 2017). Our research also utilized resources provided by the Center for Functional Neuroimaging Technologies, P41EB015896 and instruments supported by 1S10RR023401, 1S10RR019307, and 1S10RR023043 from the Athinoula A. Martinos Center for Biomedical Imaging at the Massachusetts General Hospital. Our computational work was partially performed on resources of the National Supercomputing Centre, Singapore (https://www.nscc.sg).

REFERENCES

[1] D. D. Garrett, G. R. Samanez-Larkin, S. W. S. MacDonald, U. Lindenberger, A. R. McIntosh, and C. L. Grady, "Moment-to-moment brain signal variability: a next frontier in human brain mapping?," *Neurosci. Biobehav. Rev.*, vol. 37, no. 4, pp. 610–624, 2013.

[2] D. D. Garrett, N. Kovacevic, A. R. McIntosh, and C. L. Grady, "Blood oxygen level-dependent signal variability is more than just noise," *J. Neurosci.*, vol. 30, no. 14, pp. 4914–4921, 2010.

[3] D. D. Garrett, N. Kovacevic, A. R. McIntosh, and C. L. Grady, "The importance of being variable," *J. Neurosci.*, vol. 31, no. 12, pp. 4496–4503, 2011.

[4] J. S. Nomi, T. S. Bolt, C. E. C. Ezie, L. Q. Uddin, and A. S. Heller, "Moment-to-moment BOLD signal variability reflects regional changes in neural flexibility across the lifespan," *J. Neurosci.*, vol. 37, no. 22, pp. 5539–5548, 2017.

[5] G. R. Samanez-Larkin, C. M. Kuhnen, D. J. Yoo, and B. Knutson, "Variability in nucleus accumbens activity mediates age-related suboptimal financial risk taking," *J. Neurosci.*, vol. 30, no. 4, pp. 1426–1434, 2010.

[6] D. J. N. Armbruster-Genç, K. Ueltzhöffer, and C. J. Fiebach, "Brain signal variability differentially affects cognitive flexibility and cognitive stability," *J. Neurosci.*, vol. 36, no. 14, pp. 3978–3987, 2016.

[7] P. Liang, J. Xiang, H. Liang, Z. Qi, K. Li, and Alzheimer's Disease NeuroImaging Initiative, "Altered amplitude of low-frequency fluctuations in early and late mild cognitive impairment and Alzheimer's disease," *Curr. Alzheimer Res.*, vol. 11, no. 4, pp. 389–398, 2014.

[8] R. C. Petersen, "Mild cognitive impairment as a diagnostic entity," *J. Intern. Med.*, vol. 256, no. 3, pp. 183–194, 2004.

[9] M. van der Meulen *et al.*, "Associative and semantic memory deficits in amnestic mild cognitive impairment as revealed by functional magnetic resonance imaging," *Cogn. Behav. Neurol.*, vol. 25, no. 4, pp. 195–215, 2012.

[10] J. Rissman, A. Gazzaley, and M. D'Esposito, "Measuring functional connectivity during distinct stages of a cognitive task," *NeuroImage*, vol. 23, no. 2, pp. 752–763, 2004.

[11] K. J. Friston, S. Williams, R. Howard, R. S. Frackowiak, and R. Turner, "Movement-related effects in fMRI time-series," *Magn. Reson. Med.*, vol. 35, no. 3, pp. 346–355, 1996.

[12] J. Ashburner, "A fast diffeomorphic image registration algorithm," *NeuroImage*, vol. 38, no. 1, pp. 95–113, 2007.

[13] L. Breiman, "Random forests," *Machine Learning*, vol. 45, no. 1, pp. 5–32, 2004.

[14] A. R. McIntosh and N. J. Lobaugh, "Partial least squares analysis of neuroimaging data: applications and advances," *NeuroImage*, vol. 23 Suppl 1, pp. S250-263, 2004.

[15] M. Guitart-Masip, A. Salami, D. Garrett, A. Rieckmann, U. Lindenberger, and L. Bäckman, "BOLD Variability is Related to Dopaminergic Neurotransmission and Cognitive Aging," *Cereb. Cortex*, vol. 26, no. 5, pp. 2074–2083, 2016.